### Anomalous Charm Production at Large $x_F$ 1

W.-K. Tang<sup>2</sup>
Stanford Linear Accelerator Center
Stanford University, Stanford, CA 94309

#### Abstract

We show that the new QCD production mechanisms which were proposed by S. J. Brodsky, P. Hoyer, A. H. Mueller and the author can explain at least some of the anomalous behavior of open and/or closed charm production at large  $x_F$ .

### 1 Introduction

Charm production at large  $x_F$  is a very fascinating regime which provides a lot of information about the internal structure, especially the higher Fock state components of the projectile in the question [1, 2]. No matter whether it is deep inelastic scattering, pion nucleus collisions, open charm or hidden charm production [3, 4, 5, 6, 7, 8, 11, 13, 12, 14], all of them show anomalous behavior which cannot be explained by leading twist PQCD. In fact, in the  $x \to 1$  limit, there is a new hard scale  $\Lambda^2_{QCD}/(1-x)$ , and the corrections to leading twist terms are of order  $\Lambda^2_{QCD}/(1-x)Q^2$ . Actually, in the combined limit,

the twist expansion breaks down and higher twist terms are no longer suppressed and can become dominant.

This paper is organized as follow: in section 2, we will review some of the experimental data which shows that higher twist effects are important at large  $x_F$ . It is well known that higher twist terms are suppressed by  $\mathcal{O}(1/M^2)$  so it raises the question why they become dominant at large  $x_F$ . Thus, we need to understand the physical origin of the suppression of higher twist terms at moderate  $x_F$  and this is reviewed in section 3. We then explain in section 4 why in the new limit,  $x_F \to 1$  and  $M^2 \to \infty$  but with  $\mu^2 = (1 - x_F)M^2$  fixed, higher twist terms are not suppressed. We will argue in section 5 that in this new QCD limit, the cross section for freeing the  $c\bar{c}$  pair is not small due to the fact that the dominant contribution comes from peripheral processes in which slow spectator quarks interact with the target. These new production mechanisms are then applied to different processes and can explain at least some of anomalous behavior observed. Finally, we give our conclusion in the last section.

<sup>&</sup>lt;sup>1</sup>Invited talk presented at Workshop on the Future of High Sensitivity Charm Experiments: Charm2000, Fermilab, Batavia, Il., June 7-9, 1994

<sup>&</sup>lt;sup>2</sup>Work supported by the Department of Energy, contract DE-AC03-76SF00515

# 2 Anomalous behavior of open and/or hidden charm production at large $x_F$

(a) It is reported by EMC [3] that the c(x) distribution measured at large  $x_{bj}$  is anomalously high. The CERN measurements disagree with photon-gluon fusion by a factor of 20 to 30 at  $Q^2 = 75 \text{ GeV}^2$  and  $x_{bj} = 0.422$  as shown in Fig. 1a and b. One should notice that the measured  $x_{bj}$  is the fractional longitudinal momentum for one charm quark only. The total  $x_{bj}$  for the  $c\bar{c}$  pair should be nearly double which is 0.85, very close to 1. In Fig. 1a and b, one can see that photon-gluon fusion fits the data well for  $x_{jb}$  less than 0.3, but badly for  $x_{bj}$  larger than 0.4.

Figure 1: Fig. 1a shows the value of  $F_2^{c\bar{c}}$  versus  $Q^2$  for fixed x:  $\circ$  (x=0.00422),  $\times$ (x = 0.00750),  $\triangle$ (x = 0.0133),  $\otimes$ (x = 0.0237),  $\diamond$ (x = 0.0422),  $\bullet$ (x = 0.0750),  $\square$ (x = 0.133),  $\oplus$ (x = 0.237),  $\nabla$ (x = 0.422). Please notice the large disagreement between experimental data  $\nabla$  and the PGF prediction (smooth curves). In Fig. 1b the charm quark momentum density distribution xc(x) as a function of x and  $Q^2$  is plotted. The PGF prediction (smooth curves) does not fit the data when x is large. The data is from Ref.[3].

(b) A sudden change in polarization of the  $J/\psi$  is reported by CIP [4] and E537 [5] at large  $x_F$  in  $\pi N$  collisions. The polarization of the  $J/\psi$  is determined by the angular distribution of its decay muons in the  $J/\psi$  rest frame. By rotational symmetry and parity, the angular distribution of massless muons, integrated over the azimuthal angle, has the

form

$$\frac{d\sigma}{d\cos\theta} \propto 1 + \lambda\cos^2\theta \tag{2}$$

where  $\theta$  is the angle between the  $\mu^+$  and the projectile direction (*i.e.*, in the Gottfried–Jackson frame). The parameter  $\lambda$  is directly related to the polarization of the  $J/\psi$  particle, *i.e.*,

$$\lambda = \begin{cases} 1 & \text{transverse } J/\psi \\ 0 & \text{unpolarized } J/\psi \\ -1 & \text{longitudinal } J/\psi. \end{cases}$$
 (3)

In Fig. 2, where  $\lambda$  is plotted against  $x_F$ , one can clearly see that the polarization of the produced  $J/\psi$  changes sharply from unpolarized to longitudinally polarized around  $x_F \sim 0.85$ . This dramatic effect is inconsistent with leading order QCD.

Figure 2: CIP data:  $x_F$  dependence of  $\lambda$  fitted to the  $J/\psi$  decay. Please notice the sudden change of the  $J/\psi$  polarization around  $x_F \sim 0.85$ .

(c) The measurement from NA3 [6] shows that double  $J/\psi$  pairs are hadroproduced only at large  $x_F$ . In the NA3 experiment, 6  $\psi\psi$  are found at 150 GeV and  $7\psi\psi$  at 280 GeV in  $\pi^-$  beam scattering with a platinum target. In table 1, we list the  $x_F$  of the  $\psi\psi$  pair of all 13 events in ascending order. The mean  $x_F$  of the pair is 0.71 (150 GeV) and 0.53 (280 GeV) which is very large.

The data also indicates strong correlations in the production mechanisms. The transverse momentum of the  $\psi\psi$  pair is  $0.9\pm0.1$  GeV for the 280 GeV beam; whereas uncorrelated pairs from a Monte Carlo study have a much larger mean transverse momentum of 1.7 GeV. Also amazingly, the mean value of the individual  $J/\psi$  transverse momenta in the  $\psi\psi$  events,

$P_{\pi}$	$x_F$ of $\psi\psi$ pair							
150  GeV	0.58	0.61	0.75	0.75	0.77	0.78		
280  GeV	0.39	0.47	0.47	0.48	0.51	0.65	0.75	

Table 1: The  $x_F$  of the  $\psi\psi$  pair of all 13 events in ascending order. The data are from Ref. [6].

1.5 GeV, is significantly higher than the mean transverse momentum of the  $\psi\psi$  pair, so there is strong correlation of between the transverse momenta of two  $J/\psi$ 's produced.

To make a quantitative statement about the correlation, we should compared the measured double  $J/\psi$  cross section per nucleon  $\sigma_{\psi\psi}$  with  $A^{1/3}(\sigma_{\psi}/\sigma_{tot})^2\sigma_{tot}$ , which is the theoretical estimate assuming that the  $\psi$ 's are produced uncorrelated. Here  $\sigma_{\psi}/\sigma_{tot}$  is the probability of producing a  $J/\psi$  in a pion nucleon collision. The extra  $A^{1/3}$  dependence takes into account the nuclear effect. In table 2, we compare the two cross sections and find that the theoretical prediction is off by three orders of magnitude! This strongly indicates that we need a new production mechanism in order to account for the large disagreement. The leading charm hadroproduction and the nuclear dependence, being reviewed in the following paragraphs, give us hint of the nature of this new mechanism.

	$P_{\pi}$	$\sigma_{\psi\psi}$ [pb]	$\sigma_{\psi}$ [nb]	$\sigma_{tot} \; [mb]$	$A^{1/3}(\sigma_{\psi}/\sigma_{tot})^2\sigma_{tot} [10^{-2} \text{pb}]$
	150  GeV	$18 \pm 8$	6.5	$\sim 25$	1.0
ĺ	280  GeV	$30 \pm 10$	8.7	$\sim 25$	1.7

Table 2: Cross sections per nucleon for double  $J/\psi$  production in  $\pi^-N$  collisions and the theoretical prediction assuming the  $J/\psi$ 's are produced uncorrelated. The data is from Ref. [6].

(d) Dramatic leading particle effects in hadronic D production are observed by WA82 [7] and E769 [8] experiments. In  $\pi^-(\bar{u}d)$  interactions with hadrons or nuclei, the  $D^-(\bar{c}d)$  and  $D^0(c\bar{u})$  are referred to as "leading" charm mesons while the  $D^+(c\bar{d})$  and  $\overline{D}^0(u\bar{c})$  are "nonleading". The asymmetry between leading and nonleading charm, which has been used in the analyses of the WA82 and E769 collaborations, is defined as

$$\mathcal{A} = \frac{\sigma(\text{leading}) - \sigma(\text{nonleading})}{\sigma(\text{leading}) + \sigma(\text{nonleading})} \tag{4}$$

Both experiment find that the measured  $\mathcal{A}(x_F)$  increases from  $\sim 0$  for  $x_F \leq 0.4$  to  $\sim 0.5$  around  $x_F = 0.65$  (Fig. 3). Therefore, the leading charm asymmetry is localized at large  $x_F$  only.

According to leading twist QCD, the hadroproduction cross section of D mesons is given by

$$\frac{d\sigma_{AB\to DX}}{dx_a dx_b dz_1} \propto \sum_{ab} f_{a/A}(x_a) f_{b/B}(x_b) \hat{\sigma}_{ab\to c\bar{c}} D_{D/c}(z_1). \tag{5}$$

Figure 3: Leading charm asymmetry versus  $x_F$ . A substantial asymmetry is observed at large  $x_F$ .

The structure functions of the initial hadrons,  $f_{a/A}(x_a)$ , are process independent while the fragmentation functions  $D_{D/c}(z_1)$  are independent of the quantum numbers of both the projectile and the target. Thus, leading twist QCD predicts the leading charm asymmetry to be nearly zero.<sup>3</sup> The observed large leading charm asymmetry breaks QCD factorization which strongly suggests that it is a higher twist effect.

(e) The data [11, 12, 13] on  $J/\psi$  production in hadron-nucleus collisions exhibits a surprising result. The NA3 and E772 data give direct evident for the breakdown of the leading twist approximation at large  $x_F$ . Following the argument of Ref.[14], by the factorization theorem, the cross section of  $J/\psi$  production in  $\pi A$  collisions is,

$$\frac{d\sigma_{\pi A \to J/\psi X}}{dx_1 dx_2} = f_{a/\pi}(x_1) f_{b/A}(x_2) \hat{\sigma}(ab \to J/\psi) \tag{6}$$

For simplicity we just assume gluon gluon fusion to be dominant. For  $\sqrt{s} \gg M_{\psi}^2$  and  $x_F > 0$ , approximately  $x_1 \simeq x_F$ ,  $x_2 \simeq M_{\psi}^2/x_F s$ . In the factorized formula (6), the nuclear Adependence appears only through the target function  $f_{b/A}(x_2)$ . Hence, ratios  $R = A\sigma(pp \to J/\psi + X)/\sigma(pA \to J/\psi + X)$  of  $J/\psi$  production should be independent of c.m. energies  $\sqrt{s}$  when  $\sqrt{s}$  and  $x_F$  varied in such a way as to keep  $x_2$  constant. However, as shown in Fig. 4, the NA3 data [11] shows that the ratio for H/Pt is consistent with Feynman scaling, i.e., scales with  $x_F$  but not with  $x_2$ . A clear energy dependence is seen at small values of  $x_2$ . Thus the leading twist factorization fails at large Feynman x of the  $J/\psi$ , since  $x_2 \simeq M_{\psi}^2/x_F s$ . A similar result was observed by combining pA data from NA3 and E772 [12].

The same anomalous behavior is also observed if one studies the nuclear A-dependence of the  $J/\psi$  production cross section through the parametrization  $\sigma_A = \sigma_p A^{\alpha}$ . The effective

<sup>&</sup>lt;sup>3</sup>Next-to-leading order calculation do give rise to a small charge asymmetry between  $\bar{c}$  and c production due to qg and  $q\bar{q}$  interference [9, 10].

Figure 4: The ratio  $R = A\sigma(pp \to J/\psi + X)/\sigma(pp \to J/\psi + X)$  of inclusive  $J/\psi$  production on Hydrogen and Platinum [11]. In (a) the ratio is plotted as a function of  $x_F$  of  $J/\psi$ , and in (b) as a function of  $x_2$ .

power  $\alpha$  at different energies show that indeed  $\alpha = \alpha(x_F)$ , *i.e.*, the nuclear suppression obeys Feynman scaling [12], and is not a function of  $x_2$ . The power  $\alpha$  decreases from 0.97 at  $x_F = 0$  to 0.7 as  $x_F \to 1$  [11, 12, 13] (see Fig. 5), *i.e.*, becomes surface dominated at large  $x_F$ .

The above nuclear A-dependence and the leading charm asymmetry directly contradict leading-twist PQCD factorization and suggest that higher twist effects play an important role at large  $x_F$ . But it is a well known fact that higher twist effects are suppressed by  $\mathcal{O}(1/M^2)$ . This raises the question of how the higher twist effects survive and become dominant at large  $x_F$ . In the next section we will review the physics of higher twist terms and point out a way to overcome the usual suppression.

# 3 Physical Picture of Higher Twist Terms

Let us take the well known process, Deep Inelastic Scattering (DIS), to illustrate the physics of 'leading twist' and 'higher twist' terms. In leading twist diagrams (Fig. 6a), only the active (hit) parton interacts with the external photon and there is no connection between the spectator partons and the active parton. On the other hand, there are strong interactions between the active parton and the spectator partons in higher twist diagrams (Fig. 6b).

If we take the 'infinitive momentum frame' in which the parton language is valid, the

Figure 5: The effective power  $\alpha$  of the A-dependence of  $J/\psi$  production : E789 ( $\bullet$ ) and E772 ( $\circ$ ) data.

proton is boosted to very high momentum along the z axis with four momentum given by  $P=(p+m^2/2p,\underline{0},p)$ . In this frame, the photon momentum can be taken as  $q=(Q^2p/m^2x,\underline{q},Q^2p/m^2x)$  and the virtuality of the photon is  $Q^2=\underline{q}^2$ ; i.e., the resolving power in transverse dimension. In other words, the transverse dimension of the partons that interact, directly or indirectly, with the photon is of the order of 1/Q. With the above pictures in mind, it is easy to understand why the higher twist terms are suppressed by  $1/Q^2$  in the usual Bjorken limit  $Q^2\to\infty$  with x fixed. As the interaction time  $\tau$  of the hard subprocess  $eq\to eq$  scattering is very short, only of the order of 1/Q, any interaction between the active parton and the spectator partons must occurs within this short time interval  $\tau$  and so they must be within transverse distance of  $r_\perp\sim 1/Q$  (Fig. 7). This immediately leads to the conclusion that higher twist terms are suppressed by  $1/Q^2$  as the probability of finding two partons with dimension  $1/Q^2$  within an area of  $1/Q^2$  is given by the geometrical factor  $1/Q^2R^2$ , with R the size of proton.

However, there is an exception to the above conclusion. Suppression of higher twist terms depends a lot on the size of proton, which is of order of 1 fm, much larger than the size of the parton, which is 1/Q. If somehow the initial proton or meson is already very small, of the same size as the parton, then there is no suppression. But how can that be realized? The answer to that question lies on the large x kinematic region and we will review that region in the next section.

Figure 6: DIS scattering: (a) leading twist and (b) higher twist.

Figure 7: The transverse view of the partons in the hadron in the infinite momentum frame.

# 4 The combined limit : $x \to 1$ and $Q^2 \to \infty$ with $(1-x)Q^2$ fixed

In the large x kinematic region, besides the usual hard scale  $Q^2$ , another new scale  $\Lambda_{QCD}^2/(1-x)$ , which reflects the hardness of this new limit, emerges [2, 1]. In fact, this new hard scale actually is the transverse size of the meson; i.e.,  $r_{\perp}^2 \sim (1-x)/\Lambda_{QCD}^2$ . If the two scales are comparable; i.e., taking the combined limit as in equation (1), higher twist contributions will not be suppressed assuming  $\mu^2 \sim \Lambda_{QCD}^2$ . In this new limit, higher and leading twist are of the same order,

$$\frac{1/Q^2}{r_{\perp}^2} \sim \frac{\Lambda_{QCD}^2}{(1-x)Q^2} \sim \frac{\Lambda_{QCD}^2}{\mu^2} \sim 1.$$

But how does the new hard scale  $\Lambda_{QCD}^2/(1-x)$  emerge in the limit  $x \to 1$ ? Let us consider Fig. 8 which gives the probability amplitude for the  $x \to 1$  perturbative distribution of the meson. The soft non-perturbative distribution is described by the wavefunction  $\phi(yp, n_{\perp})$  which is suppressed in the extreme kinematic limit  $y \to 0, 1$  or  $n_{\perp} \to \infty$ . The perturbative contribution comes from diagrams where one or more gluons are exchanged between the two

quarks. For simplicity, we just consider exchanging one gluon between the quarks in Fig. 8.

Figure 8: The  $x \to 1$  limit of a hadron structure function generated by perturbative gluon exchange.

The separation between the two quarks  $r_{\perp}$  can be estimated by considering the intermediate state  $q\bar{q}g$ . The virtuality of this state is given by

$$2p\Delta E_{q\bar{q}g} \simeq -\frac{m_q^2 + n_{\perp}^2}{y} - \frac{m_q^2 + k_{\perp}^2}{1 - x} - \frac{(n_{\perp} - k_{\perp})^2}{x - y}$$
$$\simeq \frac{m_q^2 + k_{\perp}^2}{1 - x}$$
(7)

when

$$n_{\perp}^2 \le \mathcal{O}(\frac{k_{\perp}^2}{1-x}). \tag{8}$$

Since  $\Delta E_{q\bar{q}g}$  is independent of  $n_{\perp}$ , the perturbative tail is

$$\int^{\frac{k_{\perp}^{2}}{1-x}} dn_{\perp} \phi(yp, n_{\perp}) \simeq \int^{\infty} dn_{\perp} \phi(yp, n_{\perp})$$

$$\simeq \phi(yp, r_{\perp} = 0)$$
(9)

which shows that the transverse distance between the two quarks is  $r_{\perp}^2 \sim (1-x)/k_{\perp}^2$ , very compact at the moment of creation. For a typical value,  $k_{\perp} \sim \Lambda_{QCD}$ , we find the new hard scale  $\Lambda_{QCD}^2/(1-x)$  as promised.

Another interesting physical quantity is the transverse distance  $R_{\perp}$  between the two quarks after the exchange of the gluon, *i.e.*, when one of the quark carries nearly all the longitudinal momentum. The life time of this intermediate state is very brief,

$$\Delta \tau \simeq \frac{1}{\Delta E_{q\bar{q}}} \simeq \frac{2p(1-x)}{k_{\perp}^2 + m_q^2} \tag{10}$$

Nevertheless, during this short life time, the 'slow' quark can move a transverse distance

$$R_{\perp} \simeq v_{\perp} \Delta \tau = \frac{k_{\perp}}{p(1-x)} \frac{2p(1-x)}{k_{\perp}^2 + m_q^2} \simeq \frac{2k_{\perp}}{k_{\perp}^2 + m_q^2}$$
 (11)

which for  $k_{\perp} = \mathcal{O}(\Lambda_{QCD})$  can be of the order of 1 fm. Hence, the specific large x kinematic region selects a very compact Fock state component of the meson at the moment of creation and then it expands very quickly to its normal size of 1 fm. The large transverse size  $R_{\perp}$  of the light quarks has a very important implication in the production of heavy quarks.

## 5 Dynamics in the new QCD Limit

In the previous section, we showed that there is a new scale  $\Lambda_{QCD}^2/(1-x)$  at large x and that the transverse size of the light quarks  $R_{\perp}$  can be as large as 1 fm. In this section, we want to exploit these properties in the production of heavy quarks at large x. As the transverse size  $R_{\perp}$  of the light quarks is very large, one can imagine that the heavy quark pair can be freed easily by deflecting the slow light quark. This phenomenon has been studied in Ref.[1] in the case of heavy quark production on nuclear target. The new limit in this case is defined by:

$$\begin{array}{c} M^2 \to \infty \\ x \to 1 \end{array} \right\} \quad \text{with } \mu^2 \equiv (1 - x)M^2 \text{ fixed}$$
 (12)

where M is the mass of the heavy quark pair. To understand the physics in this new limit, let us consider the "extrinsic" and "intrinsic" diagrams as shown in Figs 9a and 9b. In the extrinsic diagram the produced heavy quark pair couples directly to only one parton in the projectile while in the intrinsic case it couples to several.

The energy difference in the extrinsic diagram is given by

$$2p\Delta E \sim \frac{k_\perp^2}{1-x} + M^2. \tag{13}$$

The first term  $k_{\perp}^2/(1-x)$  comes from the effectively stopped light valence quarks  $q\bar{q}$  as the produced  $Q\bar{Q}$  pair carries almost all of the momentum  $(x \to 1)$  while the second term comes from the virtuality of the gluon which is of the order of the mass of the heavy quark pair. In order to get a large production cross section, the energy difference should be minimized and thus the two terms in equation (13) are of the same order, *i.e.*,

$$k_{\perp}^2 \sim (1-x)M^2 = \mu^2$$
 (14)

Now we have a very nice result. The transverse momentum square of the light quarks are of the order of  $\mu^2$  and so these states can be resolved by a target gluon of transverse momentum  $l_{\perp}$  of order of  $\mu$ . Hence the hardness of the scattering from the target is not  $M^2$  as one would expect in the leading twist calculation, but instead it is  $\mu^2 = (1-x)M^2$ . Actually, the transverse size of the stopped light quark pair is given by  $1/k_{\perp} \sim 1/\mu$ . This explains why the scattering dominantly occurs off the light quarks. Therefore, we can conclude that heavy quarks can be, and are, produced at large x by soft peripheral scattering and so the cross section is large. These new production mechanisms can help to explain the various anomalous behaviors of charm production as described in section 2.

In leading twist diagrams, the usual lowest order diagram describing the fusion process  $gg \to Q\bar{Q}$  is shown in Fig. 10. Although the size of the light quark pair is large, the heavy

Figure 9: Leading order diagrams in heavy quark production in the new limit (12): (a) extrinsic diagram and (b) intrinsic diagram.

quark pair QQ still has a small transverse size  $h_{\perp} \sim 1/M$ . A target gluon can resolve the  $Q\bar{Q}$  pair only provided that it has a commensurate wavelength, i.e.,  $l_{\perp} \sim M$  as indicated in Fig. 11. This is much large than the  $l_{\perp} \sim \mu$  required to resolve the light quarks. Hence the leading twist is actually suppressed by 1/M compared to the new mechanisms in the new limit.

One can also go through the same argument as described in the previous section and conclude that the Fock state of the projectile hadron from which the heavy pair is produced has a small transverse size  $r_{\perp}^2 \sim (1-x)/\mu^2 \sim 1/M^2$ . Because of the smallness of the transverse size, the intrinsic diagram as shown in Fig. 9b, where an extra gluon is attached to the heavy quark pair, is not suppressed relative to the extrinsic diagram Fig. 9a. Therefore, the distinction between extrinsic and intrinsic processes essentially disappears.

### 6 Applications of the New Mechanisms

Let us summarize the physics in the new limit (12) before we go on to apply it to the anomalous charm production. In the combined limit, the Fock states are very compact and small. The transverse radius square of the states has a typical value of  $(1-x)M^2$ . Because of the compactness of the Fock states, intrinsic diagrams and extrinsic diagrams are of the

Figure 10: Leading twist diagram in heavy quark production:  $gg \to Q\bar{Q}$ .

same order. But the intrinsic diagrams can numerically dominate the extrinsic contributions because of the large combinatic factor. The heavy quark pair can be freed easily by stripping away the slow light spectator quark in the projectile through an interaction with the target. The hardness scale of the collision is given by  $(1-x)M^2$ . It is a soft peripheral process and so the cross section is large. This picture can provide a QCD framework for understanding the puzzling features of the large x data mentioned in section 2:

- (a) The larger than expected charm structure function of the nucleon at large  $x_{bj}$  reported by EMC [3] can be understood by the large intrinsic charm contribution in the proton. In this case,  $Q^2 = 75 \text{ GeV}^2$  (for the data point with  $x_{bj} = 0.422$ ) is fixed and the photon can resolve the charm quark easily. But as discussed above, the intrinsic production of the charm pair at large  $x_F$  (which is nearly twice of  $x_{bj}$ ) can numerically dominate the usual extrinsic production considered in PGF calculation and boost up the charm structure function a lot.
- (b) The longitudinally polarized  $J/\psi$  at large  $x_F$  in  $\pi N$  collisions has a natural explanation by the new production mechanisms [15]. The dominant contributions to the polarization of  $J/\psi$  at large  $x_F$  are the intrinsic diagrams as shown in Fig. 11. The initial state pion valence quarks naturally have opposite helicities. There is a factor  $1/(1-x_F)$  enhancement for the emission of transversely polarized gluon with same sign of helicity as the radiated quark. Thus the two gluons coupled to the charm pair have opposite helicity. In order to form a bound state, the transverse momenta of the gluons and thus of the charm pair should be small. In that case, the initial  $J_z=0$  and thus the formed  $J/\psi$  is in longitudinally polarized state. Here, we have made the assumption that the formation of the  $J/\psi$  through the radiation of an extra gluon does not change the polarization of the charm quarks. In the large  $x_F$  limit, the radiated gluon must be soft and this justifies our assumption.

The counting rules in powers of  $1 - x_F$  are presented in Ref.[15]. The cross section for producing a longitudinally polarized (Fig. 12a) and a transversely polarized (Fig. 12b)  $J/\psi$  is proportional to  $(1-x_F)^3$  and  $(1-x_F)^4$  respectively. We find that the basic reason for the dominance of the intrinsic polarization amplitude (Fig. 12a) is that it allows two helicity flips of the heavy quarks, each contributing a power of  $M \sim 1/\sqrt{1-x_F}$  in our analysis. Thus, the longitudinal polarization of the  $J/\psi$  at large  $x_F$  is mainly due to intrinsic charm production mechanisms.

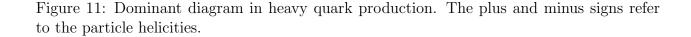


Figure 12: The production of (a) longitudinal and (b) transverse  $J/\psi$ .

- (c) The anomalous double  $J/\psi$  production can be understood qualitatively by considering intrinsic production as shown in Fig. 13. The two  $J/\psi$ 's produced as shown in the diagram clearly are strongly correlated. The cross section for freeing the pairs becomes large at large  $x_F$  as it is a soft peripheral scattering from the target. This helps to explain why the  $J/\psi$  pairs produced at large  $x_F$  only. Intrinsic charm production (Fig. 13) has another nice feature. The total transverse momentum square of the  $J/\psi$  pair is of the order of  $\mu^2 = (1-x_F)M^2$  only, i.e., of the same order as that of the light quarks. However, the individual  $J/\psi$ 's can have transverse momenta up to the mass scale M. In fact, if one uses the measured mean value of  $x_F$ , which is 0.53, from the NA3 280 GeV beam data and the measured mean transverse momentum of the individual  $J/\psi$ 's,  $M \sim k_{\perp} = 1.5$  GeV, one gets  $\mu = 1.0$  GeV which is close to the measured value of  $x_F = 0.9 \pm 0.1$  GeV. Obviously, one cannot take this number too seriously. Nevertheless, it indicates that all these features fit nicely with the data and the proposed new mechanisms may play an important role in double  $J/\psi$  production.
- (d) The leading charm asymmetry has been studied in detail by R. Vogt and S. J. Brodsky [16] using a two-component model. The first component is the usual leading twist

Figure 13: Intrinsic diagram that may account for double  $J/\psi$  production at large  $x_F$ .

fusion process while the second component is based on the model discussed above.

In the usual leading twist fusion subprocess, there is a finite probability that the produced charm quark will combine with a spectator valence quark in the final state to produce a leading hadron. Such final state coalescence mechanisms have been incorporated into PYTHIA, a Monte Carlo program based on the Lund string model [17]. In that model, the "string acceleration" of slow heavy quarks by fast valence quarks can boost the fast charm rate. However, such a mechanism overestimates the observed asymmetry  $\mathcal{A}(x_F)$  at low  $x_F$ . The Lund string model is strictly a final state coalescence. However, the model we propose is an initial state coalescence. The pion can fluctuate into higher Fock states as shown in Fig. 14. All the partons have nearly the same velocity in order to minimize the invariant mass of the state. As the charm and the valence quark have the same rapidity, it is easy for them to coalesce to form a large D meson state without paying much penalty. Thus, it can produce a strong leading particle correlation at large  $x_F$ .

Figure 14: Initial state coalescence producing a D meson through the intrinsic charm fluctuation at large  $x_F$ .

Figure 15 shows the results of the two-component model. The parameter  $\xi$  determines the relative importance of the leading twist and intrinsic charm components. All the calculations

reproduce the general trend of the data.

Figure 15: The prediction of the two-component model. The figure is from [16]

(e) The new production mechanisms have all the novel features observed in the nuclear dependence of  $J/\psi$  production. QCD factorization is invalid in the combined limit since there is no relative suppression of interactions involving several partons in the projectile. The nuclear  $A^{\alpha}$ -dependence is a function of  $x_F$  rather than a function of  $x_2$  of the target-parton momentum fraction. Because of the rapid transverse size expansion of the spectators, production cross sections in nuclear targets becomes surface dominated at large  $x_F$ .

### 7 Conclusion

We have reviewed the experimental status of charm production at large  $x_F$  and observed a lot of anomalous behaviors in this kinematic limit. Both the leading charm asymmetry and the nuclear  $J/\psi$  production show that factorization breaks down at large  $x_F$ . Higher twist effects becomes dominant because a new scale  $\Lambda_{QCD}^2/(1-x_F)$  emerges, which reflects the small transverse size of the Fock state, in the  $x \to 1$  limit. In the combined limit (12), the heavy quark pair can be freed easily as the coherence of the Fock state is easily broken by soft interactions of finite transverse momentum because of the rapid expansion of the transverse size of the spectators. This new production mechanism helps to explain the anomalous phenomena observed at large  $x_F$ . This new picture of hadrons formation opens up a whole new avenue for studying the far-off-shell structure of hadrons. It is thus critical that a new measurement of the charm and beauty structure functions be performed in future experiments.

### References

[1] S. J. Brodsky, P. Hoyer, A. H. Mueller and W.-K. Tang, Nucl. Phys. **B369**, 519 (1992).

- [2] P. Hoyer, Acta Phys.Polon. **B23**, 1145 (1992)
- [3] EMC: J. J. Aubert et al., Nucl. Phys. **B213**, 31 (1983).
- [4] CIP: C. Biino, et al., Phys. Rev. Lett. 58, 2523 (1987).
- [5] E537: C. Akerlof, et al., Phys. Rev. **D48**, 5067 (1993).
- [6] NA3: J. Badier, et al., Phys. Lett. **B114**, 457 (1982).
- [7] WA82: M. Adamovich, et al., Phys. Lett. **B305**, 402 (1993).
- [8] E769: G. A.Alves, et al., Phys. Rev. Lett. **72**, 812 (1994).
- [9] W. Beenakker, et al., Nucl. Phys. **B351**, 507 (1991).
- [10] P. Nason, S. Dawson, and R. K. Ellis, Nucl. Phys. **B327**, 49 (1989).
- [11] NA3: J. Badier, et al., Z. Phys. C20, 101 (1983).
- [12] E772: D. M. Alde, et al., Phys. Rev. Lett. 66, 133 (1991).
- [13] E789: M. S. Kowitt, et al., Phys. Rev. Lett. **72**, 1318 (1994).
- [14] P. Hoyer, M. Vänttinen and U. Sukhatme, Phys. Lett. **B246**, 217 (1990).
- [15] M. Vänttinen, P. Hoyer, S. J. Brodsky and W.-K. Tang, in preparation.
- [16] R. Vogt and S. J. Brodsky, SLAC and LBL preprint, SLAC-PUB-6468 and LBL-35380, April 1994.
- [17] H.-U. Bengtsson and T. Sjöstrand, Comput. Phys. Commun. 46, 43 (1987).

This figure "fig1-1.png" is available in "png" format from:

This figure "fig2-1.png" is available in "png" format from:

This figure "fig3-1.png" is available in "png" format from:

This figure "fig4-1.png" is available in "png" format from:

This figure "fig5-1.png" is available in "png" format from:

This figure "fig1-2.png" is available in "png" format from:

This figure "fig2-2.png" is available in "png" format from:

This figure "fig3-2.png" is available in "png" format from:

This figure "fig4-2.png" is available in "png" format from:

This figure "fig5-2.png" is available in "png" format from:

This figure "fig1-3.png" is available in "png" format from:

This figure "fig2-3.png" is available in "png" format from:

This figure "fig3-3.png" is available in "png" format from:

This figure "fig4-3.png" is available in "png" format from:

This figure "fig5-3.png" is available in "png" format from: